MA 788 — Numerical Methods for PDEs

Semidiscrete Central-Upwind Schemes for Hyperbolic Conservation Laws

Final Project Report

Gabe Cantanelli, Grayson Gall, Andrew Lys, Hayden Outlaw

Department of Mathematics, North Carolina State University, Raleigh, NC 27695

Submitted: June 8, 2026

---

1 Introduction

Consider a general multidimensional system of conservation laws, given by:

$$u_t + \nabla_{\boldsymbol{x}} \cdot f(u) = 0, \quad \boldsymbol{x} \in \mathbb{R}^d \tag{1}$$

The Godunov-type schemes for numerical solutions are projection-evolution-reconstruction methods, which are based on average values over cells (or finite volumes) in the domain. Given a piecewise constant initial condition, these methods introduce piecewise polynomial interpolants, evolve these interpolants one step forward in time, and project the evolved solution back into the form of cell averages. One has much flexibility in designing these finite volume schemes, in that one can select polynomial interpolations of varying orders of accuracy, different forward-step functions, and different methods of projection back into cell averages. Here, we will specifically focus on the central mechanism of the forward step function, which must be designed to preserve the accuracy of the polynomial interpolation, introduce minimal numerical oscillation and diffusion, be computationally efficient, converge with a desired order of accuracy, and generalize well to higher dimensions.

In this project, we reproduce the results presented in [6], in which a new semidiscrete central-upwind scheme for numerically solving the system in Equation 1 is proposed. While all schemes must make tradeoffs to reach their varied goals, this scheme serves as an extension of the classic Godunov scheme [2] in that it avoids the use of computationally intensive Riemann solvers to propagate shockwaves at cell interfaces, introduces fewer oscillations due to improved flux modeling, and provides a viable extension to higher-dimensional systems. We outline the analytical basis for the scheme in both one and two spatial dimensions in Sections 3.1 and 3.2, and reproduce some numerical results from [6] and from [9] in Section 5.

2 Godunov Central Schemes

We first motivate the formulation of semidiscrete central-upwind schemes by reviewing the related Godunov-type central schemes in one spatial dimension. For the sake of simplicity, we only consider grids uniform in both space and time, of widths Δx and Δt respectively, and use the following notation:

- $x_j = j\Delta x$
- $t^n = n\Delta t$
- $x_{j\pm\frac{1}{2}} := (j \pm 1/2)\Delta x$
- $u_j^n := u(x_j, t^n)$

We also define the sliding cell average $\overline{u}(x,t)$ over the cell $(x_{j-\frac{1}{2}}, x_{j+\frac{1}{2}})$ as

$$\overline{u}(x,t) := \frac{1}{\Delta x}\int_{I(x)} u(\xi,t)\, d\xi, \quad I(x) = \left\{\xi : |\xi - x| < \frac{\Delta x}{2}\right\} \tag{2}$$

We can then use these cell averages to reformulate the system of conservation laws (Equation 1) as

$$\overline{u}(x,t+\Delta t) = \overline{u}(x,t) - \frac{1}{\Delta x}\left[\int_{\tau=t}^{t+\Delta t} f\left(u\left(x+\frac{\Delta x}{2},\tau\right)\right) - \int_{\tau=t}^{t+\Delta t} f\left(u\left(x-\frac{\Delta x}{2},\tau\right)\right)\, d\tau\right] \tag{3}$$

We assume that at any time t^n, we have some global piecewise polynomial approximation $\tilde{u}(x,t^n)$, which is expressed in Equation 4 as

$$\tilde{u}(x,t^n) = p_j^n(x), \;\; x \in (x_{j-\frac{1}{2}}, x_{j+\frac{1}{2}}) \;\forall\, j \tag{4}$$

Though there is some flexibility in defining $\tilde{u}(x,t^n)$, namely in its order of accuracy and specific limiter choices, we will assume that it is conservative, accurate to order r, and non-oscillatory. For schemes of order two, the reconstructions $\left\{p_j^n\right\}$ are piecewise linear (examples can be found in [3] and [4]); for schemes of order three, the reconstructions will instead be piecewise quadratic, and for such schemes of equal or greater order the usage of the ENO (essentially non-oscillatory) reconstruction may be warranted. This method of reconstruction utilizes information about the approximations in neighboring cells to generate reconstructions of even higher order, although it requires the usage of smoothness indicators that may or may not be available or feasible to compute. In the 1D case, specific details are provided in [4], and for the multi-D case more details are available in [7] and [8].

The basic mechanism for Godunov-type schemes then consists of applying the update function (Equation 3) to this global polynomial solution $\tilde{u}(x,t^n)$ (Equation 4) to compute the solution at time t^{n+1} in terms of its sliding averages $\overline{u}(x,t^{n+1})$. Evaluation of these sliding averages at specific grid points then yields approximations to the cell averages at the next time step. If these evaluations are computed at $x = x_j$, i.e., inside the cell, we obtain an upwind scheme. This could potentially generate non-smooth solutions at the cell interfaces $\{x_{j+\frac{1}{2}}\}$, which would require computationally expensive solutions to Riemann shockwave problems between cells. However, if we instead choose $x = x_{j+\frac{1}{2}}$ to evaluate the cell average in Equation 3, we obtain the Godunov-type central scheme:

$$\begin{aligned}\overline{u}_{j+\frac{1}{2}}^{n+1} = {} & \frac{1}{\Delta x}\left[\int_{x_j}^{x_{j+\frac{1}{2}}} p_j^n(x)\, dx + \int_{x_{j+\frac{1}{2}}}^{x_{j+1}} p_{j+1}^n(x)\, dx\right] \\ & - \frac{\lambda}{\Delta t}\left[\int_{t^n}^{t^{n+1}} f(u(x_{j+1},t))\, dt - \int_{t^n}^{t^{n+1}} f(u(x_j,t))\, dt\right], \quad \lambda := \frac{\Delta t}{\Delta x}\end{aligned} \tag{5}$$

This scheme is advantageous because the solution is smooth in the neighborhood of the points $\{x_j\}$, which permits a discretization of the integrals involving the flux function f in Equation 5 by some quadrature formula - the necessary function values at the quadrature points could be computed with a sufficiently accurate Taylor expansion or RK method.

3 Semidiscrete Central-Upwind Schemes

In this section, we outline the formulation of central-upwind semi-discrete schemes, following closely the formulation presented in [5]. We first examine an application to a 1-D system of conservation laws, and then apply it to a multi-D system of conservation laws.

3.1 Semidiscrete Central-Upwind Schemes for 1-D Conservation Laws

Consider the 1-D system (Equation 1) of N strictly hyperbolic conservation laws, i.e., the Jacobian $\frac{\partial f}{\partial u}$ has n distinct real eigenvalues, which by convention are ordered from largest to smallest from λ_1 to λ_N. We assume that at time $t = t^n$ we have some piecewise polynomial global solution $\tilde{u}(x,t)$ (Equation 4), which could potentially have discontinuities at the cell interfaces $\{x_{j+\frac{1}{2}}\}$. These discontinuities propagate with local speeds to both the left and right, which can be approximated by

$$a^+_{j+\frac{1}{2}} := \max_{\omega \in C\left(u^-_{j+\frac{1}{2}}, u^+_{j+\frac{1}{2}}\right)} \left\{ \lambda_N \left(\frac{\partial f}{\partial u}(\omega) \right), 0 \right\} \tag{6}$$

$$a^-_{j+\frac{1}{2}} := \min_{\omega \in C\left(u^-_{j+\frac{1}{2}}, u^+_{j+\frac{1}{2}}\right)} \left\{ \lambda_1 \left(\frac{\partial f}{\partial u}(\omega) \right), 0 \right\} \tag{7}$$

Here, $C(u^-_{j+\frac{1}{2}}, u^+_{j+\frac{1}{2}})$ denotes the curve in phase space connecting the points

$$u^+_{j+\frac{1}{2}} := p_{j+1}(x_{j+\frac{1}{2}}), \;\; u^-_{j+\frac{1}{2}} := p_j(x_{j+\frac{1}{2}}) \tag{8}$$

which are the polynomial approximations evaluated at the corresponding cell interface from either side. Note that this requires a computation of the eigenvalues of the Jacobian $\frac{\partial f}{\partial u}$, which is more involved than the calculation of only its spectral radius.

Next, we define some domains on which the system is to be evolved. We first define the quantities $x_{j+\frac{1}{2},l}$ and $x_{j+\frac{1}{2},r}$ by

$$x^n_{j+\frac{1}{2},l} := x_{j+\frac{1}{2}} + \Delta t a^-_{j+\frac{1}{2}}$$
$$x^n_{j+\frac{1}{2},r} := x_{j+\frac{1}{2}} + \Delta t a^+_{j+\frac{1}{2}}$$

These represent the left and right boundaries of the Riemann fan caused by the discontinuity at x_j propagated forward in time from t^n to t^{n+1}. We can then use these to define the following *nonequal* rectangular domains:

$$\underbrace{[x^n_{j-\frac{1}{2},r}, x^n_{j+\frac{1}{2},l}] \times [t^n, t^{n+1}]}_{:=D_{\text{int}}} \qquad \underbrace{[x^n_{j+\frac{1}{2},l}, x^n_{j+\frac{1}{2},l}] \times [t^n, t^{n+1}]}_{:=D_{\text{fan}}} \tag{9}$$

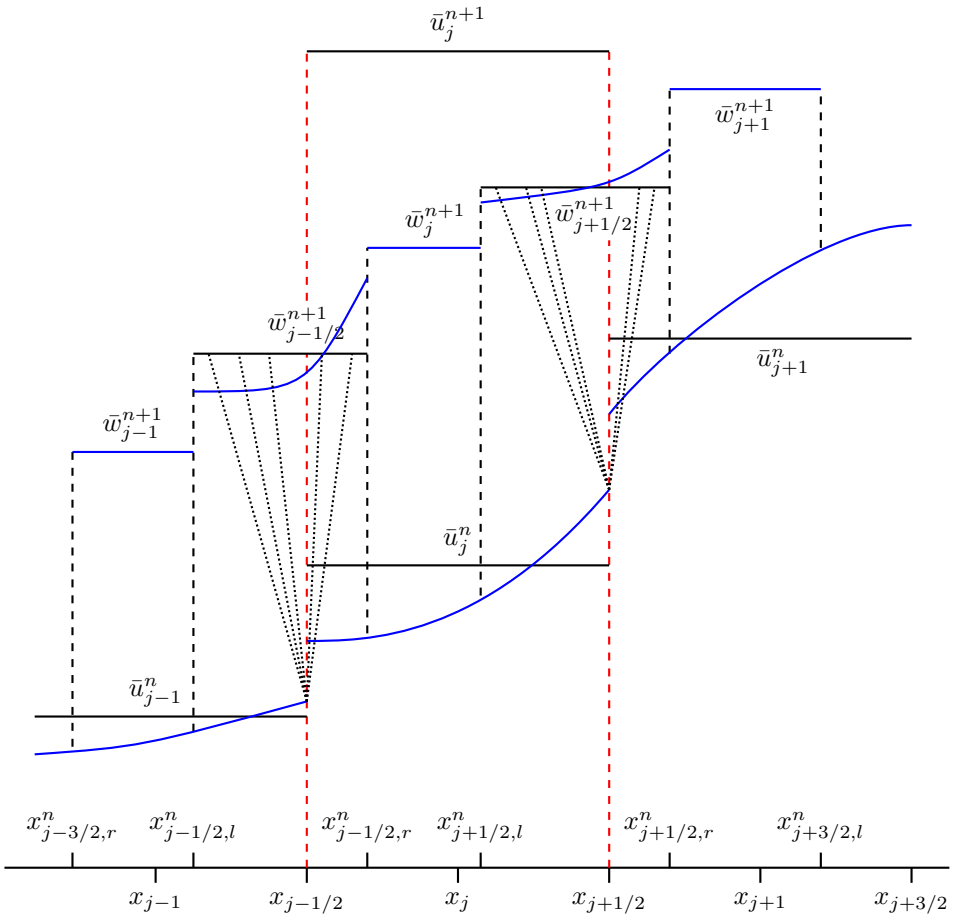

Figure 1: *1-D Semidiscrete Central-Upwind Scheme Domain*

D_{int} accounts for the evolution of the system within the cell $[x_{j-\frac{1}{2}}, x_{j+\frac{1}{2}}]$ entirely between the Riemann fans propagating at $x_{j-\frac{1}{2}}$ and $x_{j+\frac{1}{2}}$, and D_{fan} accounts for the evolution of the system within the Riemann fan propagating at $x_{j+\frac{1}{2}}$. Note that the solution $\tilde{u}(x,t^n)$ is entirely smooth within D_{int}, as it does not account for propagating discontinuities at cell interfaces; within D_{fan}, however, $\tilde{u}(x,t^n)$ is not necessarily smooth. Using both of these domains, we can then apply the update function (Equation 5) on D_{fan} and D_{int} to produce the two cell averages:

$$\overline{w}_j^{n+1} = \frac{1}{x^n_{j+\frac{1}{2},l} - x^n_{j-\frac{1}{2},r}} \left[\int_{x^n_{j-\frac{1}{2},r}}^{x^n_{j+\frac{1}{2},l}} p_j^n(x)\,dx - \int_{t^n}^{t^{n+1}} \left(f(u(x^n_{j+\frac{1}{2},l},t)) - f(u(x_{j-\frac{1}{2},r},t)) \right) dt \right] \tag{10}$$

$$\overline{w}_{j+\frac{1}{2}}^{n+1} = \frac{1}{x^n_{j+\frac{1}{2},r} - x^n_{j+\frac{1}{2},l}} \left[\int_{x_{j+\frac{1}{2},l}}^{x_{j+\frac{1}{2}}} p_j^n(x) + \int_{x_{j+\frac{1}{2}}}^{x^n_{j+\frac{1}{2},r}} p_{j+1}^n(x)\,dx - \int_{t^n}^{t^{n+1}} \left(f(u(x^n_{j+\frac{1}{2},r},t)) - f(u(x^n_{j+\frac{1}{2},l},t)) \right) dt \right] \tag{11}$$

Given a specific scheme for computing the polynomials $\{p_j^n\}$, it is possible to compute the spatial integrals in both Equation 10 and Equation 11. Since D_{fan} accounts for all of the propagation inside the Riemann fan of the shockwave, we have that the solution is smooth along line segments $(x^n_{j+\frac{1}{2},l}, t)$ and $(x^n_{j+\frac{1}{2},r}, t)$ (i.e., at the boundary of the Riemann fan) for all $t^n \le t \le t^{n+1}$. Therefore, the time integrals in Eqns. 10 and 11 can be computed using numerical quadrature. Once these are computed, we may utilize both cell averages to create the nonoscillatory, conservative, third-order polynomial interpolant, defined piecewise as

$$\tilde{w}^{n+1}(x) = \sum_j \left(\tilde{w}_j^{n+1}(x) \chi_{\left[x^n_{j-\frac{1}{2},r}, x^n_{j+\frac{1}{2},l}\right]} + \tilde{w}^{n+1}_{j+\frac{1}{2}} \chi_{\left[x^n_{j+\frac{1}{2},l}, x^n_{j+\frac{1}{2},r}\right]} \right) \tag{12}$$

Here, the χ functions are the characteristic functions of the corresponding subscripted intervals, and $\tilde{w}_j^{n+1}(x)$ and $\tilde{w}^{n+1}_{j+\frac{1}{2}}$ are the associated quadratic pieces. (Note that even for a nonuniform grid, specific piecewise quadratic reconstructions can be written explicitly.) The scheme is then finally constructed by projecting $\tilde{w}^{n+1}$ back onto the original grid by computing the cell averages:

$$\bar{u}_j^{n+1} = \frac{1}{\Delta x} \int_{x_{j-\frac{1}{2}}}^{x_{j+\frac{1}{2}}} \tilde{w}^{n+1}(x)\, dx \tag{13}$$

This defines a fully discrete Godunov-type central-upwind scheme, which can be derived explicitly (see [6]).

3.1.1 Expression in Conservative Form

Using the definition in Equation 13, the time derivative of $\overline{u}_j(t)$ is

$$\frac{d}{dt}\overline{u}_j(t) = \lim_{\Delta t \to 0} \frac{\overline{u}_j^{n+1} - \overline{u}_j^n}{\Delta t} = \lim_{\Delta t \to 0} \frac{1}{\Delta t} \left[\frac{1}{\Delta x} \int_{x_{j-\frac{1}{2}}}^{x_{j+\frac{1}{2}}} \tilde{w}^{n+1}(x)\, dx - \overline{u}_j^n \right] \tag{14}$$

Now, suppose that the slopes of $\tilde{w}^{n+1}_{j\pm\frac{1}{2}}$ are uniformly bounded, independently of Δt. Since the width of each Riemann fan is bounded above by $(a^+_{j+\frac{1}{2}} - a^-_{j+\frac{1}{2}})\Delta t$, we can create the approximation

$$\tilde{w}^{n+1}_{j\pm\frac{1}{2}}(x) = \overline{w}^{n+1}_{j\pm\frac{1}{2}} + \mathcal{O}(\Delta t) \quad \forall x \in \left[x^n_{j\pm\frac{1}{2},l}, x^n_{j\pm\frac{1}{2},r} \right] \tag{15}$$

Since the reconstruction is conservative, it also holds that

$$\frac{1}{x^n_{j+\frac{1}{2},l} - x^n_{j-\frac{1}{2},r}} \int_{x^n_{j-\frac{1}{2},r}}^{x^n_{j+\frac{1}{2},l}} \tilde{w}_j^{n+1}(x) dx = \bar{w}_j^{n+1} \tag{16}$$

i.e, that the process of projecting the third order piecewise polynomial interpolant back to original cell averages is a first order operation with respect to time. Combining Equations 14, 15, and 16, as well as the definitions of $x^n_{j-\frac{1}{2},r}$ and $x^n_{j+\frac{1}{2},l}$, we have

$$\frac{d}{dt}\overline{u}_j(t) = \frac{a^+_{j-\frac{1}{2}}}{\Delta x} \lim_{\Delta t \to 0} \overline{w}^{n+1}_{j-\frac{1}{2}} + \lim_{\Delta t \to 0} \frac{1}{\Delta t} \left(\frac{x^n_{j+\frac{1}{2},l} - x^n_{j-\frac{1}{2},r}}{\Delta x} \overline{w}_j^{n+1} - \overline{u}_j^n \right) - \frac{a^-_{j+\frac{1}{2}}}{\Delta x} \lim_{\Delta t \to 0} \overline{w}^{n+1}_{j+\frac{1}{2}} \tag{17}$$

To address the three limits in time in Equation 17 separately, we first have via Equations 10 and 11[1]:

[1] As in Equation 8, $u^{\pm}_{j+\frac{1}{2}}$ denote the right and left values of the piecewise polynomial interpolant $\{p_j\}$ at time t.

$$\lim_{\Delta t\to 0}\frac{1}{\Delta t}\left(\frac{x^n_{j+\frac{1}{2},l}-x^n_{j-\frac{1}{2},r}}{\Delta x}\overline{w}^{n+1}_j-\overline{u}^n_j\right)=\frac{a^-_{j+\frac{1}{2}}u^-_{j+\frac{1}{2}}-a^+_{j-\frac{1}{2}}u^+_{j-\frac{1}{2}}}{\Delta x}-\frac{f(u^-_{j+\frac{1}{2}})-f(u^+_{j-\frac{1}{2}})}{\Delta x} \tag{18}$$

$$\lim_{\Delta t\to 0}\overline{w}^{n+1}_{j+\frac{1}{2}}=\frac{a^+_{j+\frac{1}{2}}u^+_{j+\frac{1}{2}}-a^-_{j+\frac{1}{2}}u^-_{j+\frac{1}{2}}}{a^+_{j+\frac{1}{2}}-a^-_{j+\frac{1}{2}}}-\frac{f(u^+_{j+\frac{1}{2}})-f(u^-_{j+\frac{1}{2}})}{a^+_{j+\frac{1}{2}}-a^-_{j+\frac{1}{2}}} \tag{19}$$

Combining Equations 18 and 19 into Equation 17, we can thus express the scheme in the following conservative form:

$$\frac{d}{dt}\overline{u}_j(t)=-\frac{H_{j+\frac{1}{2}}(t)-H_{j-\frac{1}{2}}(t)}{\Delta x} \tag{20}$$

where the numerical fluxes $H_{j+\frac{1}{2}}$ are given by

$$H_{j+\frac{1}{2}}(t):=\frac{a^+_{j+\frac{1}{2}}f(u^-_{j+\frac{1}{2}})-a^-_{j+\frac{1}{2}}f(u^+_{j+\frac{1}{2}})}{a^+_{j+\frac{1}{2}}-a^-_{j+\frac{1}{2}}}+\frac{a^+_{j+\frac{1}{2}}a^-_{j+\frac{1}{2}}}{a^+_{j+\frac{1}{2}}-a^-_{j+\frac{1}{2}}}\left(u^+_{j+\frac{1}{2}}-u^-_{j+\frac{1}{2}}\right) \tag{21}$$

3.1.2 Properties of the 1-D Semidiscrete Scheme

First, as a critical advantage over upwind schemes, the semidiscrete scheme defined by Equations 20 and 21 is a Godunov-type central scheme. The use of integration over Riemann fans that propagate from cell interfaces does not require expensive Riemann solvers for shockwave propagation. Furthermore, the numerical viscosity of the scheme is independent of $\mathcal{O}(1/\Delta t)$, which demonstrates that the scheme is suitable for steady-state calculations. The more accurate estimation of the width of the Riemann fans[2] also reduces the effect of numerical dissipation.

Now, note that if we take

$$a^+_{j+\frac{1}{2}}=-a^-_{j+\frac{1}{2}}=\max_{\omega\in C\left(u^{n-}_{j+\frac{1}{2}},u^{n+}_{j+\frac{1}{2}}\right)}\rho\left(\frac{\partial f}{\partial u}(\omega)\right):=a_{j+\frac{1}{2}} \tag{22}$$

i.e., a one-sided propagation speed estimate, then Equation 21 reduces to

$$H_{j+\frac{1}{2}}(t):=\frac{f(u^+_{j+\frac{1}{2}})-f(u^-_{j+\frac{1}{2}})}{2}-\frac{a_{j+\frac{1}{2}}}{2}\left(u^+_{j+\frac{1}{2}}-u^-_{j+\frac{1}{2}}\right) \tag{23}$$

This numerical flux reduces further if one assumes that f is monotone. Without loss of generality, if $f'(u)\geq 0$, then $a^-_{j+\frac{1}{2}}=0$ for all j, in which case the scheme simplifies to the standard upwind scheme:

$$\frac{d}{dt}u_j(t)=-\frac{f(u^n_j)-f(u^n_{j-1})}{\Delta x} \tag{24}$$

(This motivates the naming of the scheme as *central-upwind*.) Equation 24 represents a system of time-dependent ODEs, which can be solved by any numerically stable ODE solver (of accuracy greater than or equal to the spatial accuracy of the scheme).

In addition, in the case of a scalar conservation law and the generalized min-mod limiter, we have that the scheme defined by Equations 20 and 21 is TVD. Namely,

$$\tilde{u}^n_j=\bar{u}^n_j+\sigma^n_j(x-x_j) \tag{25}$$

[2]using the specific eigenvalues of the system Jacobian, as opposed to only its spectral radius.

where

$$\sigma_j^n = \text{minmod}\left(\theta\frac{\bar{u}_j^n - \bar{u}_{j-1}^n}{\Delta x}, \frac{\bar{u}_{j+1}^n - \bar{u}_{j-1}^n}{2\Delta x}, \theta\frac{\bar{u}_{j+1}^n - \bar{u}_j^n}{\Delta x}\right) \tag{26}$$

and $\theta \in [1, 2]$. We are done if we show the hypotheses of the following lemma, due to [11], are satisfied.

Lemma 1. *The scheme given by (20) is TVD, if we have:*

$$H_{j+1/2}(t) \geq f(u_j(t)) \geq H_{j-1/2}(t) \qquad \textit{when } u_j(t) \textit{ is a local maximum} \tag{27}$$

and

$$H_{j+1/2}(t) \leq f(u_j(t)) \leq H_{j-1/2}(t) \qquad \textit{when } u_j(t) \textit{ is a local minimum} \tag{28}$$

To begin, we have the following for $\overline{u}_{j+1/2}^{n,\pm}$ with the min-mod reconstruction:

$$\overline{u}_{j+1/2}^{n,-} = \overline{u}_j^n + \frac{\Delta x}{2}\sigma_j^n$$
$$\overline{u}_{j+1/2}^{n,+} = \overline{u}_{j+1}^n - \frac{\Delta x}{2}\sigma_{j+1}^n$$

Focusing on u, we claim that if u_j is a local maximum, then $u_{j-1/2}^-, u_{j+1/2}^+ \leq u_j$. We only prove this for $u_{j+1/2}^+$ since the other case is similar. Since u_j is a local maximum, we have that $u_{j+1} - u_j \leq 0$ so, by definition of the min-mod limiter, either $u_{j+1/2}^+ = u_{j+1} \leq u_j$, or $u_{j+2} < u_{j+1} < u_j$. In this latter case, we have

$$\sigma_{j+1} = \max\left(\theta\frac{u_{j+1} - u_j}{\Delta x}, \frac{u_{j+2} - u_j}{2\Delta x}, \theta\frac{u_{j+2} - u_{j+1}}{\Delta x}\right)$$

Namely, $\sigma_{j+1} \geq \frac{\theta}{\Delta x}(u_{j+1} - u_j)$. Recalling that $\theta \leq 2$, we have

$$\frac{\Delta x}{2}\sigma_{j+1} \geq \frac{\theta}{2}(u_{j+1} - u_j) \geq u_{j+1} - u_j$$

which proves that $u_j \geq u_{j+1/2}^+$. If u_j is a local maximum, we have the following simplifications for $u_{j-1/2}^+$ and $u^- = u_{j+1/2}^-$. First, $\text{sign}(u_j - u_{j-1}) \neq \text{sign}(u_{j+1} - u_j)$ so that $\sigma_j = 0$. This immediately gives us

$$u_{j+1/2}^- = u_j \qquad \text{and} \qquad u_{j-1/2}^+ = u_j$$

Now, we look at $H_{j+1/2} - f(u_j) = H_{j+1/2} - f(u^-)$. Plugging in the definition of $H_{j+1/2}$, we have

$$H_{j+1/2} - f(u_j) = -\frac{a^-}{a^+ - a^-}\left[f(u^+) - f(u^-) - a^+(u^+ - u^-)\right]$$

where $u^+ = u_{j+1/2}^+$. Now, by the mean value theorem, we take ω between u^- and u^+, giving us that the right hand side

$$= -\frac{a^-}{a^+ - a^-}\left[(f'(\omega) - a^+)(u^+ - u^-)\right]$$

The following four facts serve as the coup de grâce:

$$a^- \leq 0 \qquad a^+ \geq 0 \qquad f'(\omega) \leq a^+ \qquad u^- = u_j \geq u^+$$

We then have that the right hand side is non-negative, so that indeed $H_{j+1/2} \geq f(u_j)$. Showing the other inequality is identical, subtracting $f(u^+)$ instead of $f(u^-)$, and the case of the local minimum follows almost identically.

Now, we quickly prove the initial lemma, following [11].

Proof. Taking the forward difference of (20), we have:

$$\frac{d}{dt}\Delta u_{j+1/2} = -\frac{1}{\Delta x}(H_{j+3/2} - H_{j+1/2}) + \frac{1}{\Delta}(H_{j+1/2} - H_{j-1/2})$$

Now, we multiple both sides by $\text{sign}(\Delta u_{j+1/2})$ and sum over j, giving us

$$\frac{d}{dt}TV(u) = \sum_j \frac{1}{\Delta x}(\text{sign}(\Delta u_{j+1/2}) - \text{sign}(\Delta u_{j-1/2}))(H_{j+1/2} - H_{j-1/2})$$

If we have that each term on the right hand side is non-positive, then we are done. The only non-zero terms are those where $\text{sign}(\Delta u_{j+1/2}) \neq \text{sign}(\Delta u_{j-1/2})$. In this case, we have that u_j is a local extremum. Therefore, for this to hold we require:

$$\begin{aligned} H_{j+1/2} &\geq H_{j-1/2} \qquad u_j \text{ is a local maximum} \\ H_{j+1/2} &\leq H_{j-1/2} \qquad u_j \text{ is a local minimum} \end{aligned}$$

Which holds if we have the hypotheses of the lemma. □

What we have obtained is, in fact, a slight strengthening of the lemma as initially stated, but this is immaterial.

3.2 Semidiscrete Central-Upwind Schemes for multi-D Conservation Laws

The scheme presented in Section 3.1 (Equations 20 and 21) can be readily generalized to a higher-dimensional case. Without loss of generality, consider the 2-D conservation law

$$u_t + f(u)_x + g(u)_y = 0 \tag{29}$$

We can then make use of the two-dimensional grid defined by

- $x_j := j\Delta x$
- $x_{j\pm\frac{1}{2}} := x_j \pm \frac{\Delta x}{2}$
- $y_k := k\Delta y$
- $y_{k\pm\frac{1}{2}} := y_k \pm \frac{\Delta y}{2}$

and where we let $\chi_{j,k}$ be the characteristic function for $[x_{j-\frac{1}{2}}, x_{j+\frac{1}{2}}] \times [y_{k-\frac{1}{2}}, y_{k+\frac{1}{2}}]$. We again assume that we start at time $t = t^n$ with a conservative piecewise polynomial reconstruction of a sufficient order of accuracy:

$$\tilde{u}^n(x,y) := \sum_{j,k} p^n_{j,k}(x,y)\chi_{j,k} \tag{30}$$

We then define key point values as follows:

- $u_{j,k} := p^n_{j,k}(x_j, y_k)$
- $u^E_{j,k} := p^n_{j,k}(x_{j+\frac{1}{2}}, y_k)$
- $u^{NW}_{j,k} := p^n_{j,k}(x_{j-\frac{1}{2}}, y_{k+\frac{1}{2}})$
- $u^N_{j,k} := p^n_{j,k}(x_j, y_{k+\frac{1}{2}})$
- $u^W_{j,k} := p^n_{j,k}(x_{j-\frac{1}{2}}, y_k)$
- $u^{SE}_{j,k} := p^n_{j,k}(x_{j+\frac{1}{2}}, y_{k-\frac{1}{2}})$
- $u^S_{j,k} := p^n_{j,k}(x_j, y_{k-\frac{1}{2}})$
- $u^{NE}_{j,k} := p^n_{j,k}(x_{j+\frac{1}{2}}, y_{k+\frac{1}{2}})$
- $u^{SW}_{j,k} := p^n_{j,k}(x_{j-\frac{1}{2}}, y_{k-\frac{1}{2}})$

As well as the cell averages:

$$\overline{u}_{j,k} := \frac{1}{\Delta x \Delta y} \int_{x_{j-\frac{1}{2}}}^{x_{j+\frac{1}{2}}} \int_{y_{k-\frac{1}{2}}}^{y_{k+\frac{1}{2}}} p_{j,k}^n(x,y)\, dxdy \tag{31}$$

As with the 1D case, the polynomial interpolant $\tilde{u}^n(x,y,t^n)$ may have discontinuities at the cell interfaces, but now the interface has four different edges, given by $x = x_{j\pm\frac{1}{2}}$ and $y = y_{k\pm\frac{1}{2}}$. Estimating the speed at which these discontinuities propagate exactly is nontrivial, but we can use a generalization of the 1D Riemann fans to estimate the local speeds of propagation as follows:

$$\begin{aligned}
a^+_{j+\frac{1}{2},k} &:= \max\left\{\lambda_N\left(\frac{\partial f}{\partial u}(u^W_{j+1,k})\right), \lambda_N\left(\frac{\partial f}{\partial u}(u^E_{j,k})\right), 0\right\} \\
b^+_{j,k+\frac{1}{2}} &:= \max\left\{\lambda_N\left(\frac{\partial g}{\partial u}(u^S_{j,k+1})\right), \lambda_N\left(\frac{\partial g}{\partial u}(u^N_{j,k})\right), 0\right\} \\
a^-_{j+\frac{1}{2},k} &:= \min\left\{\lambda_1\left(\frac{\partial f}{\partial u}(u^W_{j+1,k})\right), \lambda_1\left(\frac{\partial f}{\partial u}(u^E_{j,k})\right), 0\right\} \\
b^-_{j,k+\frac{1}{2}} &:= \min\left\{\lambda_1\left(\frac{\partial g}{\partial u}(u^S_{j,k+1})\right), \lambda_1\left(\frac{\partial g}{\partial u}(u^N_{j,k})\right), 0\right\}
\end{aligned} \tag{32}$$

We also consider four separate nonuniform domains, which are defined by

$$\begin{aligned}
D_{j,k+\frac{1}{2}} &:= [x_{j-\frac{1}{2}} + A^+_{j-\frac{1}{2},k+\frac{1}{2}}\Delta t, x_{j+\frac{1}{2}} + A^-_{j+\frac{1}{2},k+\frac{1}{2}}\Delta t] \times [y_{k+\frac{1}{2}} + b^-_{j,k+\frac{1}{2}}\Delta t, y_{k+\frac{1}{2}} + b^+_{j,k+\frac{1}{2}}\Delta t], \\
D_{j+\frac{1}{2},k} &:= [x_{j+\frac{1}{2}} + a^-_{j+\frac{1}{2},k}\Delta t, x_{j+\frac{1}{2}} + a^+_{j+\frac{1}{2},k}\Delta t] \times [y_{k-\frac{1}{2}} + B^+_{j+\frac{1}{2},k-\frac{1}{2}}\Delta t, y_{k+\frac{1}{2}} + B^-_{j+\frac{1}{2},k+\frac{1}{2}}\Delta t] \\
D_{j+\frac{1}{2},k+\frac{1}{2}} &:= [x_{j+\frac{1}{2}} + A^-_{j+\frac{1}{2},k+\frac{1}{2}}\Delta t, x_{j+\frac{1}{2}} + A^+_{j+\frac{1}{2},k+\frac{1}{2}}\Delta t] \times [y_{k+\frac{1}{2}} + B^-_{j+\frac{1}{2},k+\frac{1}{2}}\Delta t, y_{k+\frac{1}{2}} + B^+_{j+\frac{1}{2},k+\frac{1}{2}}\Delta t] \\
D_{j,k} &:= [x_{j-\frac{1}{2}}, x_{j+\frac{1}{2}}] \times [y_{k-\frac{1}{2}}, y_{k+\frac{1}{2}}] \setminus \bigcup_{\pm} [D_{j,k\pm\frac{1}{2}} \cup D_{j\pm\frac{1}{2},k} \cup D_{j\pm\frac{1}{2},k\pm\frac{1}{2}}]
\end{aligned} \tag{33}$$

where

$$\begin{aligned}
A^+_{j+\frac{1}{2},k+\frac{1}{2}} &:= \max\left\{a^+_{j+\frac{1}{2},k}, a^+_{j+\frac{1}{2},k+1}\right\} \\
A^-_{j+\frac{1}{2},k+\frac{1}{2}} &:= \min\left\{a^-_{j+\frac{1}{2},k}, a^-_{j+\frac{1}{2},k+1}\right\} \\
B^+_{j+\frac{1}{2},k+\frac{1}{2}} &:= \max\left\{b^+_{j,k+\frac{1}{2}}, b^+_{j+1,k+\frac{1}{2}}\right\} \\
B^-_{j+\frac{1}{2},k+\frac{1}{2}} &:= \min\left\{b^-_{j,k+\frac{1}{2}}, b^-_{j+1,k+\frac{1}{2}}\right\}
\end{aligned} \tag{34}$$

As with the 1D case, under a suitable CFL condition the solution to the 2D conservation law (Equation 29) with initial condition $\tilde{u}$ is smooth in the central domain $D_{j,k}$ away from the Riemann fans, and non-smooth within the others. Note that $D_{j,k}$ is *not* in general a rectangular domain as the system evolves.

Integrating the conservation law (29) over the domains in time and space:

$$D_{j,k} \times [t^n, t^{n+1}], D_{j\pm\frac{1}{2},k} \times [t^n, t^{n+1}], D_{j,k\pm\frac{1}{2}} \times [t^n, t^{n+1}], D_{j\pm\frac{1}{2},k\pm\frac{1}{2}} \times [t^n, t^{n+1}]$$

thus creates new cell averages for each domain, namely $\{\overline{w}^{n+1}_{j,k+\frac{1}{2}}\}, \{\overline{w}^{n+1}_{j+\frac{1}{2},k}\}, \{\overline{w}^{n+1}_{j+\frac{1}{2},k+\frac{1}{2}}\}$, and $\{\overline{w}^{n+1}_{j,k}\}$. Analogous to the 1-D case, we then use them to produce a two-dimensional piecewise polynomial reconstruction:

$$\tilde{w}^{n+1}(x,y) := \sum_{j,k} \left[\tilde{w}^{n+1}_{j,k} \tilde{\chi}_{j,k}(x,y) + \tilde{w}^{n+1}_{j+\frac{1}{2},k} \tilde{\chi}_{j+\frac{1}{2},k}(x,y) + \tilde{w}^{n+1}_{j,k+\frac{1}{2}} \tilde{\chi}_{j,k+\frac{1}{2}}(x,y) + \tilde{w}^{n+1}_{j+\frac{1}{2},k+\frac{1}{2}} \tilde{\chi}_{j+\frac{1}{2},k+\frac{1}{2}}(x,y) \right] \tag{35}$$

where again as in Equation 12, the $\tilde{w}$'s denote the quadratic interpolation components and $\tilde{\chi}$'s are the corresponding characteristic functions for each domain. To complete the forward step, we then project the interpolant given by Equation 35 back onto the original 2-D grid:

$$\overline{u}^{n+1}_{j,k} = \frac{1}{\Delta x \Delta y} \int_{x_{j-\frac{1}{2}}}^{x_{j+\frac{1}{2}}} \int_{y_{k-\frac{1}{2}}}^{y_{k+\frac{1}{2}}} \tilde{w}^{n+1}(x,y)\, dxdy \tag{36}$$

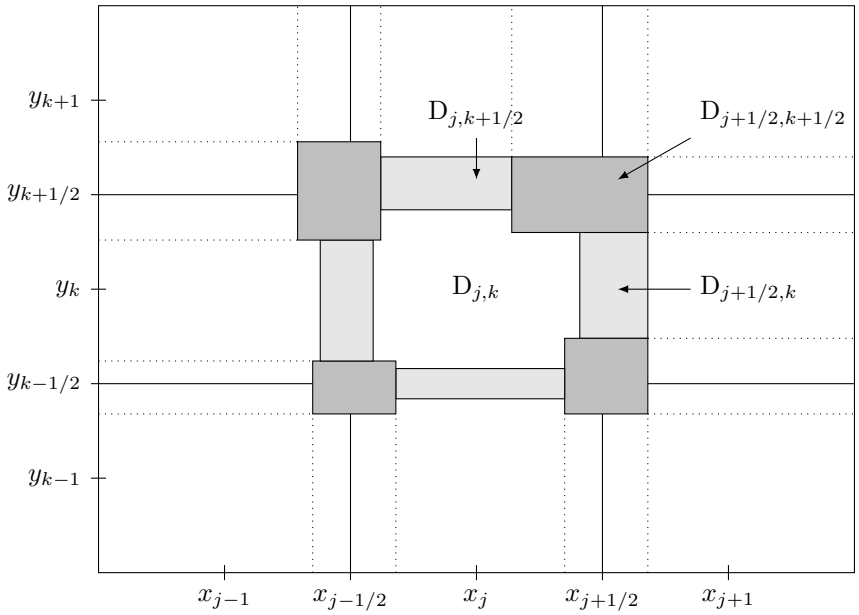

Figure 2: *2-D Semidiscrete Central-Upwind Scheme Domain*

3.2.1 Expression in Conservative Form

We can again express the 2-D scheme in conservative form within the semidiscrete framework. We first set the following notation for the various intersections of the cells $[x_{j-\frac{1}{2}}, x_{j+\frac{1}{2}}] \times [y_{k-\frac{1}{2}}, y_{k+\frac{1}{2}}]$ with the domains D: $C_{j\pm\frac{1}{2},k\pm\frac{1}{2}}$ for the four corners, $S_{j\pm\frac{1}{2},k}$ and $S_{j,k\pm\frac{1}{2}}$ for the four side domains, and $D_{j,k}$ for the center. The sizes of these component domains are $|C| \approx (\Delta t)^2$ and $|S| \approx \Delta t$. If we again assume that the spatial derivatives of $\tilde{w}^{n+1}$ are bounded independently of Δt, we can relate the polynomial interpolation and cell averages as:

$$\int\int_{C_{j\pm\frac{1}{2},k\pm\frac{1}{2}}} \tilde{w}^{n+1}_{j\pm\frac{1}{2},k\pm\frac{1}{2}}\, dxdy = \mathcal{O}(\Delta t^2) \tag{37}$$

$$\int\int_{S_{j\pm\frac{1}{2},k}} \tilde{w}^{n+1}_{j\pm\frac{1}{2},k} dxdy = |S_{j\pm\frac{1}{2},k}|\, \overline{w}^{n+1}_{j\pm\frac{1}{2},k} + \mathcal{O}(\Delta t^2) \tag{38}$$

$$\int\int_{S_{j,k\pm\frac{1}{2}}} \tilde{w}^{n+1}_{j,k\pm\frac{1}{2}} dxdy = |S_{j,k\pm\frac{1}{2}}|\, \overline{w}^{n+1}_{j,k\pm\frac{1}{2}} + \mathcal{O}(\Delta t^2) \tag{39}$$

Since we assume the reconstruction $\tilde{w}^{n+1}$ to be conservative, we additionally have:

$$\int\int_{D_{j,k}} \tilde{w}^{n+1}_{j,k}(x,y)\, dxdy = |D_{j,k}| \overline{w}^{n+1}_{j,k} \tag{40}$$

Substituting Equations 37, 38, 39, and 40 into Equation 36, we can conclude:

$$\begin{aligned}\frac{d}{dt}\overline{u}_{j,k}(t) &= \lim_{\Delta t\to 0} \frac{\overline{u}^{n+1}_{j,k} - \overline{u}^{n}_{j,k}}{\Delta t} \\ &= \lim_{t\to 0}\left(\sum_{\pm} \frac{|S_{j,k\pm\frac{1}{2}}|}{\Delta t\Delta x\Delta y}\overline{w}^{n+1}_{j,k\pm\frac{1}{2}} + \sum_{\pm}\frac{|S_{j\pm\frac{1}{2},k}|}{\Delta t\Delta x\Delta y}\overline{w}^{n+1}_{j\pm\frac{1}{2},k}\right) + \lim_{\Delta t\to 0}\frac{1}{\Delta t}\left(\frac{|D_{j,k}|}{\Delta x\Delta y}\overline{w}^{n+1}_{j,k} - \overline{u}^{n}_{j,k}\right)\end{aligned} \tag{41}$$

To calculate the limits of these sums, we assume the usage of Simpson's quadrature to integrate over $D_{j\pm\frac{1}{2},k\pm\frac{1}{2}}$ to compute $\overline{w}_{j\pm\frac{1}{2},k\pm\frac{1}{2}}$. Addressing the first sum, since $|S_{j,k\pm\frac{1}{2}}| = \mp b^{\mp}_{j,k\pm\frac{1}{2}}\Delta t\Delta x + \mathcal{O}(\Delta t^2)$, we obtain

$$\begin{aligned}\lim_{\Delta t\to 0}\frac{|S_{j,k\pm\frac{1}{2}}|}{\Delta t\Delta x\Delta y}\overline{w}^{n+1}_{j,k\pm\frac{1}{2}} \approx &-\frac{b^{+}_{j,k\pm\frac{1}{2}}b^{-}_{j,k\pm\frac{1}{2}}}{6\left(b^{+}_{j,k\pm\frac{1}{2}} - b^{-}_{j,k\pm\frac{1}{2}}\right)\Delta y}\left[u^{SW(NW)}_{j,k\pm1} + 4u^{S(N)}_{j,k\pm1} + u^{SE(NE)}_{j,k\pm1}\right] \\ &+ \frac{\left(b^{\mp}_{j,k\pm\frac{1}{2}}\right)^2}{6\left(b^{+}_{j,k\pm\frac{1}{2}} - b^{-}_{j,k\pm\frac{1}{2}}\right)\Delta y}\left[u^{NW(SW)}_{j,k} + 4u^{N(S)}_{j,k} + u^{NE(SE)}_{j,k}\right] + \frac{b^{\mp}_{j,k\pm\frac{1}{2}}}{6\left(b^{+}_{j,k\pm\frac{1}{2}} - b^{-}_{j,k\pm\frac{1}{2}}\right)\Delta y} \\ &\cdot\left[g\left(u^{SW(NW)}_{j,k\pm1}\right) - g\left(u^{NW(SW)}_{j,k}\right) + 4\left(g\left(u^{S(N)}_{j,k\pm1}\right) - g\left(u^{N(S)}_{j,k}\right)\right) + g\left(u^{SE(NE)}_{j,k\pm1}\right) - g\left(u^{NE(SE)}_{j,k}\right)\right]\end{aligned} \tag{42}$$

Similarly, we can apply the same quadrature and reduction to the second sum to conclude that

$$\begin{aligned}\lim_{\Delta t\to 0}\frac{|S_{j\pm\frac{1}{2},k}|}{\Delta t\Delta x\Delta y}\overline{w}^{n+1}_{j\pm\frac{1}{2},k} \approx &-\frac{a^{+}_{j\pm\frac{1}{2},k}a^{-}_{j\pm\frac{1}{2},k}}{6\left(a^{+}_{j\pm\frac{1}{2},k} - a^{-}_{j\pm\frac{1}{2},k}\right)\Delta x}\left[u^{NW(NE)}_{j\pm1,k} + 4u^{W(E)}_{j\pm1,k} + u^{SW(SE)}_{j\pm1,k}\right] \\ &+ \frac{\left(a^{\mp}_{j\pm\frac{1}{2},k}\right)^2}{6\left(a^{+}_{j\pm\frac{1}{2},k} - a^{-}_{j\pm\frac{1}{2},k}\right)\Delta x}\left[u^{NE(NW)}_{j,k} + 4u^{E(W)}_{j,k} + u^{SE(SW)}_{j,k}\right] + \frac{a^{\mp}_{j\pm\frac{1}{2},k}}{6\left(a^{+}_{j\pm\frac{1}{2},k} - a^{-}_{j\pm\frac{1}{2},k}\right)\Delta x} \\ &\cdot\left[f\left(u^{NW(NE)}_{j\pm1,k}\right) - f\left(u^{NE(NW)}_{j,k}\right) + 4\left(f\left(u^{W(E)}_{j\pm1,k}\right) - f\left(u^{E(W)}_{j,k}\right)\right) + f\left(u^{SW(SE)}_{j\pm1,k}\right) - f\left(u^{SE(SW)}_{j,k}\right)\right]\end{aligned} \tag{43}$$

Finally, for the last limit in Equation 41, we can use the fact that $D_{j,k}$ becomes rectangular as $\Delta t \to 0$ – the small corners are $\mathcal{O}(\Delta t^2)$ and are thus negligible. We can integrate the conservation law (Equation 29) in the same way using Simpson's rule over $D_{j,k} \times [t^n, t^n + \Delta t]$, which results in:

$$\lim_{\Delta t\to 0}\frac{1}{\Delta t}\left[\frac{|D_{j,k}|}{\Delta x\Delta y}\overline{w}_{j,k}^{n+1}-\overline{u}_{j,k}^{n}\right]\approx \frac{a^{-}_{j+\frac{1}{2},k}}{6\Delta x}\left[u^{NE}_{j,k}+4u^{E}_{j,k}+u^{SE}_{j,k}\right]-\frac{a^{+}_{j-\frac{1}{2},k}}{6\Delta x}\left[u^{NW}_{j,k}+4u^{W}_{j,k}+u^{SW}_{j,k}\right]$$
$$-\frac{b^{-}_{j,k+\frac{1}{2}}}{6\Delta y}\left[u^{NW}_{j,k}+4u^{N}_{j,k}+u^{NE}_{j,k}\right]-\frac{b^{+}_{j,k-\frac{1}{2}}}{6\Delta y}\left[u^{SW}_{j,k}+4u^{S}_{j,k}+u^{SE}_{j,k}\right]$$
$$-\frac{1}{6\Delta x}\left[f(u^{NE}_{j,k})-f(u^{NW}_{j,k})+4\left(f(u^{E}_{j,k})-f(u^{W}_{j,k})\right)+f(u^{SE}_{j,k})-f(u^{SW}_{j,k})\right]$$
$$-\frac{1}{6\Delta y}\left[g(u^{NW}_{j,k})-g(u^{SW}_{j,k})+4\left(g(u^{N}_{j,k})-g(u^{S}_{j,k})\right)+g(u^{NE}_{j,k})-g(u^{SE}_{j,k})\right] \tag{44}$$

We thus obtain our 2-D semidiscrete central-upwind scheme by substituting Equations (42)-(44) into Equation (41). Doing so yields the following conservative form:

$$\frac{d}{dt}\bar{u}_{j,k}(t)=-\frac{H^{x}_{j+\frac{1}{2},k}(t)-H^{x}_{j-\frac{1}{2},k}(t)}{\Delta x}-\frac{H^{y}_{j,k+\frac{1}{2}}(t)-H^{y}_{j,k-\frac{1}{2}}(t)}{\Delta y} \tag{45}$$

where the corresponding numerical fluxes are given by

$$H^{x}_{j+\frac{1}{2},k}=\frac{a^{+}_{j+\frac{1}{2},k}}{6\left(a^{+}_{j+\frac{1}{2},k}-a^{-}_{j+\frac{1}{2},k}\right)}\left[f(u^{NE}_{j,k})+4f(u^{E}_{j,k})+f(u^{SE}_{j,k})\right]$$
$$-\frac{a^{-}_{j+\frac{1}{2},k}}{6\left(a^{+}_{j+\frac{1}{2},k}-a^{-}_{j+\frac{1}{2},k}\right)}\left[f(u^{NW}_{j+1,k})+4f(u^{W}_{j+1,k})+f(u^{SW}_{j+1,k})\right]$$
$$+\frac{a^{+}_{j+\frac{1}{2},k}a^{-}_{j+\frac{1}{2},k}}{6\left(a^{+}_{j+\frac{1}{2},k}-a^{-}_{j+\frac{1}{2},k}\right)}\left[u^{NW}_{j+1,k}-u^{NE}_{j,k}+4(u^{W}_{j+1,k}-u^{E}_{j,k})+u^{SW}_{j+1,k}-u^{SE}_{j,k}\right]$$

and

$$H^{y}_{j,k+\frac{1}{2}}=\frac{b^{+}_{j,k+\frac{1}{2}}}{6\left(b^{+}_{j,k+\frac{1}{2}}-b^{-}_{j,k+\frac{1}{2}}\right)}\left[g(u^{NW}_{j,k})+4g(u^{N}_{j,k})+g(u^{NE}_{j,k})\right]$$
$$-\frac{b^{-}_{j,k+\frac{1}{2}}}{6\left(b^{+}_{j,k+\frac{1}{2}}-b^{-}_{j,k+\frac{1}{2}}\right)}\left[g(u^{SW}_{j,k+1})+4g(u^{S}_{j,k+1})+g(u^{SE}_{j,k+1})\right]$$
$$+\frac{b^{+}_{j,k+\frac{1}{2}}b^{-}_{j,k+\frac{1}{2}}}{6\left(b^{+}_{j,k+\frac{1}{2}}-b^{-}_{j,k+\frac{1}{2}}\right)}\left[u^{SW}_{j,k+1}-u^{NW}_{j,k}+4(u^{S}_{j,k+1}-u^{N}_{j,k})+u^{SE}_{j,k+1}-u^{NE}_{j,k}\right]$$

which completely specifies the multidimensional framework.

4 Implementation Details

We apply the semidiscrete central-upwind scheme to four separate cases: the 1-D Burgers' equation, the 1-D Euler equations with periodic boundary conditions and a smooth initial condition the 1-D Euler equations with solid wall boundary conditions and a discontinuous initial condition, and the 2-D Euler equations. We present an overview of the problem setup, and results replicating the experiments described by Kurganov et. al. , in [5], and by Micalizzi et. at [10].

In all experiments a second order SSP Runge-Kutta (SSP-RK2) time integrator is used and it is described in Equation 47. This method is in line with multiple other finite volume method implementations. Strong stability preserving methods reduce numerical oscillation by maintaining the property of decreasing total variation (TVD) for a sufficiently small time step, although they may require more memory and computation time as compared to traditional Runge-Kutta methods.

$$\overline{u}^{(1)} = \overline{u}^{n} + \Delta t\, \mathcal{O}\left(\overline{u}^{n}\right) \tag{46}$$

$$\overline{u}^{n+1} = \frac{1}{2}\overline{u}^{n} + \frac{1}{2}\overline{u}^{(1)} + \frac{1}{2}\Delta t\, \mathcal{O}\left(\overline{u}^{(1)}\right) \tag{47}$$

Additionally, in all cases, we use the generalized minmod limiter to reconstruct cell boundary values. The slope along direction d is given by

$$\sigma^{n}_{j,d} = \text{minmod}\left(\theta\frac{\overline{u}^{n}_{j} - \overline{u}^{n}_{j-1}}{\Delta_d}, \frac{\overline{u}^{n}_{j+1} - \overline{u}^{n}_{j-1}}{2\Delta_d}, \theta\frac{\overline{u}^{n}_{j+1} - \overline{u}^{n}_{j}}{\Delta_d}\right) \quad \theta \in [1,2], \tag{48}$$

where Δ_d is the cell width along direction d, and

$$\text{minmod}\left(z_1, ..., z_k\right) = \begin{cases} \text{sign}\left(z_1\right)\min_{1\leq l\leq k}\left(|z_l|\right) & \text{sign}\left(z_1\right) = ... = \text{sign}\left(z_k\right) \\ 0 & \text{Otherwise} \end{cases}. \tag{49}$$

In all cases presented a value of $\theta = 2$ is utilized. The value at the left cell boundary, when reconstruction is done along the x axis, and at the lower boundary, along the y axis, is given by

$$u^{+}_{j-1/2} = \overline{u}_j - \frac{\Delta_d}{2}\sigma^{n}_{j,d}, \tag{50}$$

and the value at right cell boundary, when reconstructing along the x axis, and at the upper boundary, when reconstructing along the y axis

$$u^{-}_{j+1/2} = \overline{u}_j + \frac{\Delta_d}{2}\sigma^{n}_{j,d}, \tag{51}$$

Additionally, adaptive time stepping is utilized, and the time step is selected such that the appropriate CFL condition is satisfied. The time is estimated as

$$\Delta t^{n+1} = C_{\text{CFL}} \min_{\Omega}\left(\min_{d}\left(\frac{\Delta_d}{s_d}\right),\right) \tag{52}$$

where $\min_{\Omega}$ represents the minimum value over all cells, $\min_d$ represents the minimum value over all directions, and C_{CFL} is the fraction of the stability condition desired $C_{\text{CFL}} = 1$ means the time step is selected to be at the stability limit. When solving Burgers' equation the local wave speed is estimated as

$$s_d = |u_d|, \tag{53}$$

and for the Euler equations the local wave speed is estimated as

$$s_d = |u_d| + \sqrt{\gamma \frac{p}{\rho}} \tag{54}$$

where u_d is the fluid velocity along direction d. This method of time step estimation and local wave speed estimation, for the Euler system, is the same as the one used by Micalizzi et. al. [10].

5 Numerical Experiments

5.1 1-D Burgers' Equation

pressure clip violates conservation, we do have access to vorticity exact solution, what happens if $\theta < 2$, run solid wall case farther forwards in time

The general (viscid) Burgers' equation in one spatial dimension is given by the partial differential equation

$$u_t + \frac{\partial}{\partial x}\left(\frac{1}{2}u^2\right) = \kappa u_{xx} \tag{55}$$

where $\kappa \geq 0$ is a diffusion constant. This equation captures the effects of both value-modulated advection and diffusion in its evolution of the prescribed initial data over time, and is fundamental in the study of the analytic properties of PDEs. By neglecting the diffusion term above (i.e, by taking $\kappa = 0$), one can obtain the *inviscid* Burgers' equation

$$u_t + \frac{\partial}{\partial x}\left(\frac{1}{2}u^2\right) = 0 \tag{56}$$

Despite its simplistic form, this equation serves as one of the most basic examples of a shock-producing evolution equation. Indeed, it is able to develop and propagate non-smooth or entirely discontinuous solutions from initial data that may otherwise be smooth. As a result, it also serves as a fundamental benchmark in the development of robust numerical methods for nonlinear PDEs, as significant challenges arise in addressing this behavior. Such challenges include the avoidance of spurious oscillations within computed solutions, as well as the propagation of shocks in the correct manner.

Now, observe that the inviscid equation can be expressed equivalently as

$$u_t + f(u)_x = 0$$

where $f(u) = \frac{1}{2}u^2$ is the corresponding flux function. This demonstrates that the inviscid equation is a hyperbolic conservation law, and is thus suitable for the numerical methods described here. It is worth noting that the more general viscid equation is instead parabolic on account of its nonzero diffusive term (though the numerical solution of such equations is typically handled more easily).

5.1.1 Experiment

For the Burgers' equation, equation 56, we replicate *1-D Problems : Example 1* presented by Kurganov et. al [5, pp. 725 - 726]. In this problem a periodic system on the domain $x \in [0, 2\pi]$ is subject to a sinusoidal initial condition

$$u(x, 0) = 0.5 + \sin(x). \tag{57}$$

With this setup a shock develops at time $t = 1$. To ensure that our implementation demonstrates the expected order of accuracy, second order, solutions are compared at time $t = 0.5$, at this point the solution is still smooth. The time step is estimated by taking $C_{\text{CFL}} = 0.95$.

To ensure that the expected order of accuracy is observed, a convergence study is completed. A reference solution is computed with a 10240 cell spatial discretization. Solutions are computed with eight other spatial discretizations, starting with 20 cells and doubling the number of cells until a 2560 cell discretization is used. Then, the l^1 errors between the reference solution and each discretization are computed.

We see that the implementation produces accurate physical solutions from all tested step sizes Δx, as depicted in Figure 3a. While difficult to discern from this comparison, this accuracy is made clearer by examining the l^1 errors of the computed solutions, which are depicted in Figure 3b. Past $\Delta x < 0.001$, these absolute errors are below machine precision (10^{-6}) across the entire domain, and the errors seem to converge uniformly to 0 as $\Delta x \to 0$. Furthermore, we can see that the rate of convergence is $\mathcal{O}(\Delta x^2)$ in Figure 4, which indicates a successful reproduction of the experiment implemented in [6].

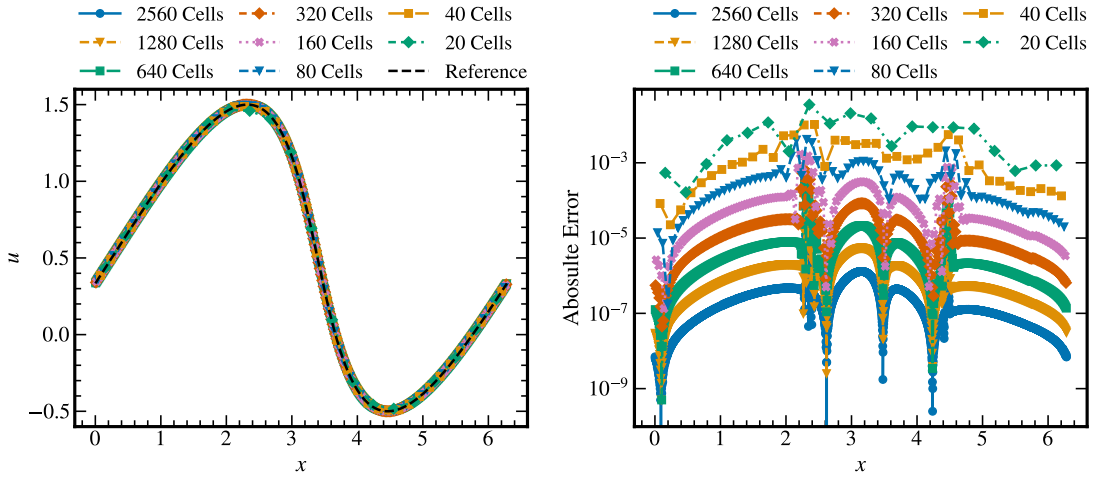

(a) *Reconstructed Solution* (b) *Absolute l^1 Error*

Figure 3: *Reconstruction and Absolute Error across Discretizations, Burgers' Equation*

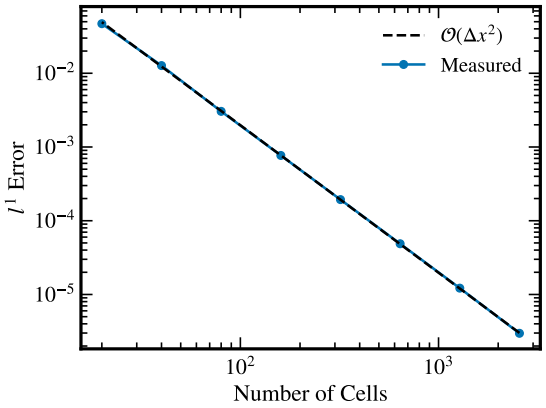

(a)

Cells	l^1 Errors	Rate
20	4.7004×10^{-2}	-
40	1.2708×10^{-2}	1.89
80	3.0426×10^{-3}	2.06
160	7.6836×10^{-4}	1.99
320	1.9345×10^{-4}	1.99
640	4.8747×10^{-5}	1.99
1280	1.2184×10^{-5}	2.00
2560	2.9750×10^{-6}	2.03

(b)

Figure 4: *Reconstruction Convergence Rate, Inviscid Burgers' Equation*

5.2 1-D Euler Equations for Gas Dynamics

Euler's equations of gas dynamics in one spatial dimension are given by the following system of conservation laws:

$$\begin{aligned} \rho_t + (\rho v)_x &= 0 \\ (\rho v)_t + \left(\rho v^2 + p\right)_x &= 0 \\ E_t + (v\,(E+p))_x &= 0 \end{aligned}$$

where ρ, v, and E are the density, velocity, and total energy of the fluid, $p = (\gamma - 1)(E - \frac{\rho}{2}v^2)$ is the pressure, and γ is the corresponding adiabatic constant (which we take to be $\gamma = 1.4$ in all test cases). As can be observed, we take our vector of conserved quantities in this formulation to be $\mathbf{u} = [\rho, m, E]^\top$, where $m = \rho v$ is the momentum of the fluid. Writing the Euler system in terms of these conserved quantities yields a system which can be written as:

$$\mathbf{u}_t + \begin{bmatrix} f_1(\mathbf{u}) \\ f_2(\mathbf{u}) \\ f_3(\mathbf{u}) \end{bmatrix}_x = 0.$$

The corresponding components of the flux are given by

$$\begin{aligned} f_1(\mathbf{u}) &= m \\ f_2(\mathbf{u}) &= \frac{m^2}{\rho} + (\gamma - 1)\left(E - \frac{m^2}{2\rho}\right) \\ f_3(\mathbf{u}) &= \frac{mE}{\rho} + (\gamma - 1)\left(\frac{mE}{\rho} - \frac{m^3}{2\rho^2}\right). \end{aligned}$$

To compute the Jacobian $\nabla f(\mathbf{u})$ in order to verify that the system is hyperbolic, (i.e, that the three eigenvalues of $\nabla f(\mathbf{u})$ are real numbers, independent of $\mathbf{u}$ and γ), it follows from straightforward algebraic manipulations of the second and third components of the flux that

$$\begin{aligned} f_2(\mathbf{u}) &= (3-\gamma)\frac{m^2}{2\rho} + (\gamma - 1)E \\ f_3(\mathbf{u}) &= \gamma\frac{mE}{\rho} + (1-\gamma)\frac{m^3}{2\rho^2} \end{aligned}$$

With this, we can compute the elements of $\nabla f(\mathbf{u})$ as follows:

- $\dfrac{\partial f_1}{\partial \rho} = 0$
- $\dfrac{\partial f_1}{\partial m} = 1$
- $\dfrac{\partial f_1}{\partial E} = 0$
- $\dfrac{\partial f_2}{\partial \rho} = \dfrac{(\gamma-3)m^2}{2\rho^2}$
- $\dfrac{\partial f_2}{\partial m} = \dfrac{(3-\gamma)m}{\rho}$
- $\dfrac{\partial f_2}{\partial E} = \gamma - 1$
- $\dfrac{\partial f_3}{\partial \rho} = \dfrac{(\gamma-1)m^3}{\rho^3} - \dfrac{\gamma m E}{\rho^2}$
- $\dfrac{\partial f_3}{\partial m} = \dfrac{\gamma E}{\rho} + \dfrac{3(1-\gamma)m^2}{2\rho^2}$
- $\dfrac{\partial f_3}{\partial E} = \dfrac{\gamma m}{\rho}$

As such, we can express $\nabla f(\mathbf{u})$ as

$$\nabla f(\mathbf{u}) = \begin{bmatrix} 0 & 1 & 0 \\ \dfrac{(\gamma-3)}{2}r_1^2 & -(\gamma-3)r_1 & \gamma - 1 \\ (\gamma-1)r_1^3 - \gamma r_1 r_2 & \gamma r_2 - \dfrac{3(\gamma-1)}{2}r_1^2 & \gamma r_1 \end{bmatrix}$$

where we have taken $r_1 = m/\rho$ and $r_2 = E/\rho$ accordingly. One can use this form of the Jacobian to verify that its eigenvalues are indeed real, which demonstrates that the system is hyperbolic and is thus suitable for these numerical methods also. Note that in the special case of an ideal gas (in which $\gamma = 1.4$), the Jacobian reduces to

$$\nabla f(\mathbf{u}) = \begin{bmatrix} 0 & 1 & 0 \\ -0.8r_1^2 & 1.6r_1 & 0.4 \\ 0.4r_1^3 - 1.4r_1 r_2 & -0.6r_1^2 + 1.4r_2 & 1.4r_1 \end{bmatrix}$$

5.2.1 Experiment 1

As a first test of the implementation of the 1-D Euler solver, we replicate the case *5.1.1 Advection of smooth density* from presented by Micalizzi and Toro [10]. This is another periodic system on the domain $x \in [-1, 1]$ subject to a smooth initial condition,

$$\mathbf{u}(x,0) = \begin{bmatrix} \rho(x,0) \\ v(x,0) \\ p(x,0) \end{bmatrix} = \begin{bmatrix} 2 + \sin^4(\pi x) \\ v_\infty \\ p_\infty \end{bmatrix} \tag{58}$$

that represents the advection of a density profile over the domain. The system is evolved in time until $t = 2$, and again a value of $C_{CFL} = 0.95$ is used to estimate the time step.

This initial data corresponds to pure advection of the density profile at a uniform rightward speed of $v_\infty = 1$, as well as a uniform pressure of $p_\infty = 1$. The exact solution of this case is given by $\mathbf{u}(x,t) = \mathbf{u}(x-t,0)$. Though this configuration is relatively simple, capturing this pure advection within an upwind scheme can prove to be quite challenging, as such schemes have the tendency to introduce excessive smoothing of the initial profile and suffer from a loss of accuracy/resolution over time. As such, this case serves as a good performance benchmark for our central-upwind method and allows for comparison against a known solution. Again, eight spatial discretizations are considered, the same number of cells as used for the Burgers' case. Both the solutions and spatially resolved errors for the density at time $t = 2$ are reported in Figure 5. The l^1 error for each grid as well as a table of errors and convergence rates are presented in Figure 6.

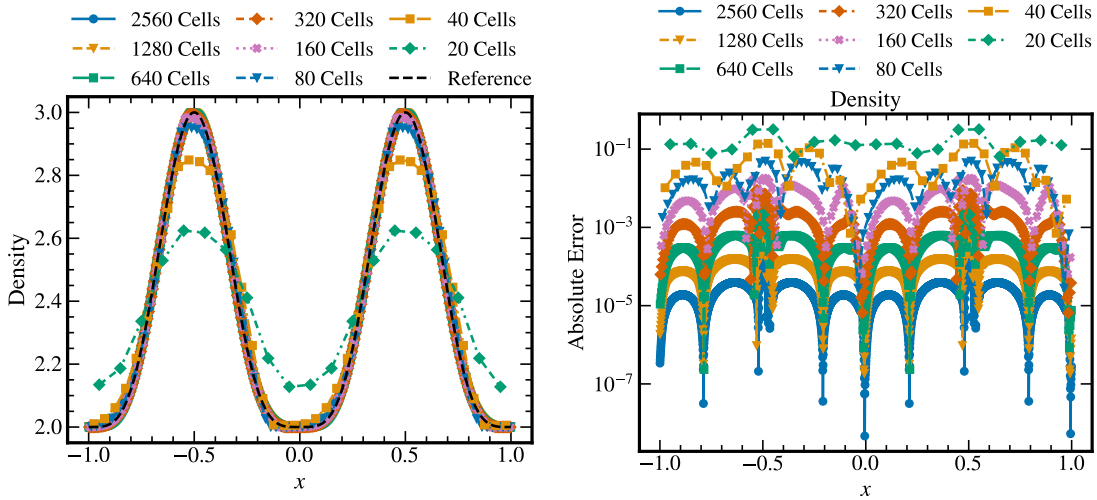

(a) *Reconstructed Solution*

(b) *Absolute ℓ^1 Error*

Figure 5: *Reconstruction and Absolute Error Across Discretizations, 1D-Euler Equations, Periodic IC*

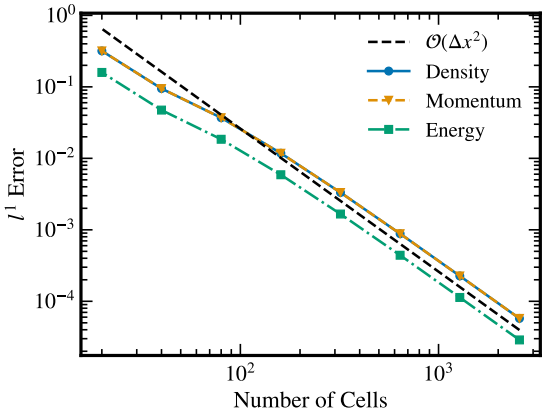

(a)

Cells	l^1 Error	Rate
20	3.1825	-
40	9.4637×10^{-2}	1.75
80	3.6957×10^{-2}	1.36
160	1.1786×10^{-2}	1.65
320	3.3259×10^{-3}	1.83
640	8.8165×10^{-4}	1.92
1280	2.2632×10^{-4}	1.96
2560	5.7643×10^{-5}	1.97

(b)

Figure 6: *Smooth Density Advection Errors*

In these results we see that our implementation achieves the expected second-order accuracy in its estimation of the conserved quantities with respect to the l^1 error. While only results are presented for the density, the analysis was repeated for all other quantities with consistent results.

5.2.2 Experiment 2

As a second test of the implementation of the 1-D Euler solver, we replicate the case *1-D Euler equations of gas dynamics* presented by presented by Kurganov et. al. [5]. We model Euler's equations of gas dynamics in 1-D on the domain $x \in [0, 1]$, using the following initial values for the conserved variables:

$$\mathbf{u}(x,0) = \begin{bmatrix} \mathbf{u}_L \\ \mathbf{u}_C \\ \mathbf{u}_R \end{bmatrix} = \begin{cases} [1, 0, 2500]^T, & \text{if } 0 \leq x < 0.1, \\ [1, 0, 0.025]^T, & \text{if } 0.1 \leq x < 0.9, \\ [1, 0, 250]^T, & \text{if } 0.9 \leq x < 1. \end{cases} \tag{59}$$

This represents an initial configuration of uniform (unit) density, zero momentum, and staggered energies. We also apply the "solid wall" boundary conditions at both endpoints of the interval. This condition is comprised of "no flux" boundary conditions for density and energy, and "reflective" boundary conditions for momentum. In practice, there are multiple ways that one can implement these solid wall conditions - here, we implement them by setting the ghost cells to the following values:

$$\begin{aligned} \rho_{-2} &= \rho_1 & \rho_{-1} &= \rho_0 \\ \rho_N &= \rho_{N-1} & \rho_{N+1} &= \rho_{N-2} \\ E_{-2} &= E_1 & E_{-1} &= E_0 \\ E_N &= E_{N-1} & E_{N+1} &= E_{N-2} \\ u_{-2} &= -u_1 & u_{-1} &= -u_0 \\ u_N &= -u_{N-1} & u_{N+1} &= -u_{N-2} \end{aligned}$$

where negative indices represent the ghost cells to the left of the domain, and indices greater than $N-1$ represent the ghost cells to the right of the domain. We evolve the system until the final time $t = 0.01$. In the original work, solutions using both 400 and 1600 cells are presented, and we repeat this as well. In order to perform a direct comparison to the original case, we plot our results superimposed over those

presented in Figures 4.1, 4.2, and 4.3 of the original work. Our results are in color, while the results from the original work are in black. These results are presented in Figure 7.

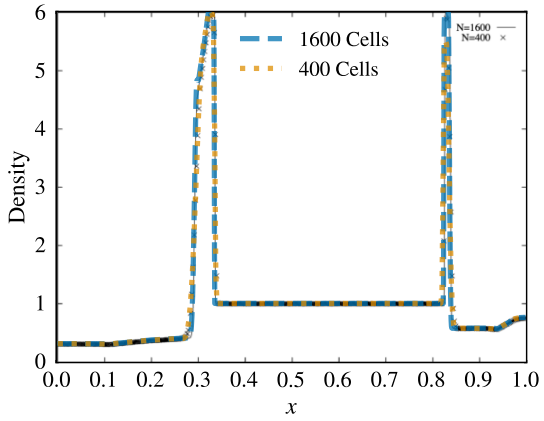

(a) *Reconstructed Density (ρ)*

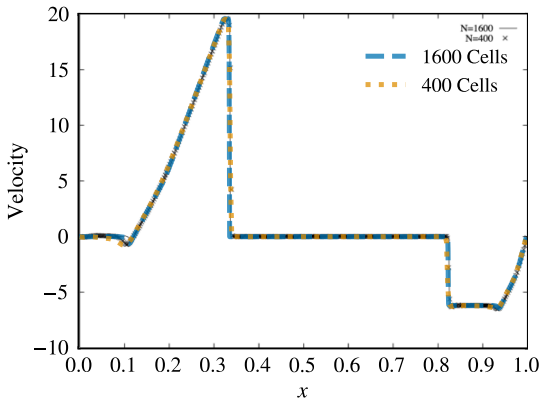

(b) *Reconstructed Velocity (u)*

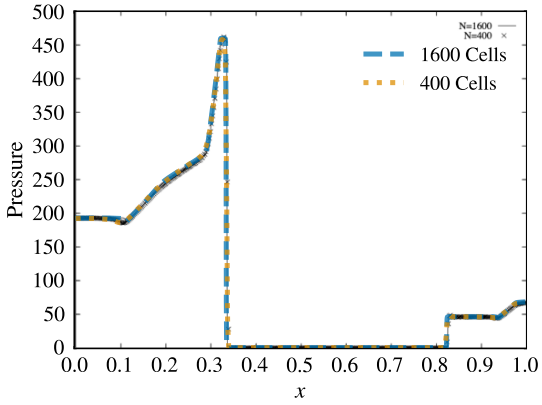

(c) *Reconstructed Pressure p*

Figure 7: *Reconstructed Conserved Variables, Implementation and Reference, ([6]), 1D Solid Wall*

Figure 7 shows that our implementation produces results that are consistent with those presented by Kurganov et. al. Is it important to note, however, that our implementation is only second order , while their implementation is third order.

When implementing the scheme, we encountered large oscillations and non-physical solutions. Eventually, we discovered the source of the issues to lie in the reconstruction. Since we use a second order reconstruction, the linear term can result in negative pressure. This is a well-known problem with the second order semi-discrete central-upwind scheme [1], which we solve in the following way. After reconstruction, and after each stage of time integration, each cell is checked for a negative value of pressure. If a negative pressure is encountered in reconstruction, then we set the approximate derivative equal to zero. Similarly, during the time evolution, if a negative pressure is encountered we default to the previously computed value. This patch may be less theoretically motivated, since where this happens the scheme is locally of order zero, but it is useful enough in reproducing sufficiently physical results.

5.3 2-D Euler Equations for Gas Dynamics

The Euler equations in two spatial dimensions can be obtained via a straightforward generalization of the one-dimensional case, and are given by the following system of four conservation laws:

$$\begin{aligned}
\rho_t + (\rho v)_x + (\rho w)_y &= 0 \\
(\rho v)_t + (\rho v^2 + p)_x + (\rho v w)_y &= 0 \\
(\rho w)_t + (\rho v w)_x + (\rho w^2 + p)_y &= 0 \\
E_t + (v(E+p))_x + (w(E+p))_y &= 0
\end{aligned}$$

Here, ρ and E are as before, but v and w now represent the x- and y- components of the velocity $\mathbf{v} = [v, w]^\top$. The pressure p is now computed as

$$p = (\gamma - 1)\left(E - \frac{\rho}{2}(v^2 + w^2)\right)$$

Analogous to the 1D case, we now take our vector of conserved variables to be $\mathbf{u} = \begin{bmatrix}\rho & m_1 & m_2 & E\end{bmatrix}^\top$, where $m_1 = \rho v$ and $m_2 = \rho w$ represent the components of the momentum. With this, we can express the system in terms of the conserved variables as

$$\mathbf{u}_t + \begin{bmatrix} f_1(\mathbf{u}) \\ f_2(\mathbf{u}) \\ f_3(\mathbf{u}) \\ f_4(\mathbf{u}) \end{bmatrix}_x + \begin{bmatrix} g_1(\mathbf{u}) \\ g_2(\mathbf{u}) \\ g_3(\mathbf{u}) \\ g_4(\mathbf{u}) \end{bmatrix}_y = 0$$

where the components of the flux functions are given by

- $f_1(\mathbf{u}) = m_1$
- $f_2(\mathbf{u}) = \dfrac{m_1^2}{\rho} + (\gamma - 1)\left(E - \dfrac{1}{2\rho}(m_1^2 + m_2^2)\right)$
- $f_3(\mathbf{u}) = \dfrac{m_1 m_2}{\rho}$
- $f_4(\mathbf{u}) = \dfrac{m_1}{\rho}\left(E + (\gamma - 1)(E - \dfrac{1}{2\rho}(m_1^2 + m_2^2))\right)$
- $g_1(\mathbf{u}) = m_2$
- $g_2(\mathbf{u}) = \dfrac{m_1 m_2}{\rho}$
- $g_3(\mathbf{u}) = \dfrac{m_2^2}{\rho} + (\gamma - 1)\left(E - \dfrac{1}{2\rho}(m_1^2 + m_2^2)\right)$
- $g_4(\mathbf{u}) = \dfrac{m_2}{\rho}\left(E + (\gamma - 1)(E - \dfrac{1}{2\rho}(m_1^2 + m_2^2))\right)$

It is important to note that the Euler equations (in any number of spatial dimensions) serve as a limiting case of the more general Navier-Stokes equations of fluid dynamics. More precisely, they can be obtained from the Navier-Stokes equations via the assumption that the flow is both inviscid and adiabatic, i.e, that the fluid has no viscosity and no thermal conductivity. This limits the applicability of the model to regimes in which this "perfect fluid" assumption is valid. Note that the flow is allowed to be compressible - if incompressibility is assumed, one can replace the relevant energy equation with one specifying that the flow is divergence-free.

5.3.1 Experiment

As a test of the implementation of the 2-D Euler solver, we replicate the case *5.2.1 Smooth isentropic unsteady vortex* presented by Micalizzi et. al. [9]. The 2D Euler system is solved on a two dimensional

periodic domain, $\Omega = [-10, 10] \times [-10, 10]$, subject to the initial data

$$\mathbf{u}(x, y, 0) = \begin{bmatrix} \rho(x, y, 0) \\ v(x, y, 0) \\ w(x, y, 0) \\ p(x, y, 0) \end{bmatrix} = \begin{bmatrix} (1 + \delta T)^{(\gamma-1)^{-1}} \\ v_\infty - \frac{\beta}{2\pi} \exp\left(\frac{1-r^2}{2}\right)(y - y_c) \\ w_\infty + \frac{\beta}{2\pi} \exp\left(\frac{1-r^2}{2}\right)(x - x_c) \\ (1 + \delta T)^{\gamma(\gamma-1)^{-1}} \end{bmatrix}$$

where

$$\delta T = -\frac{(\gamma - 1)\beta^2}{8\gamma\pi^2} \exp\left(1 - r^2\right)$$
$$r = \sqrt{(x - x_c)^2 + (y - y_c)^2}$$

and $\beta = 5$. We take $[x_c, y_c]^\top = [0, 0]^\top$ to be the center of the vortex, and $[v_\infty, w_\infty]^\top = [1, 1]^\top$ to be the fluid velocity infinitely far from the vortex center. The system is evolved until time $t = 0.1$ and a value of $C_{\text{CFL}} = 0.95$ is once again utilized.

Using this problem setup a convergence study was performed. The reference solution was generated using a 2560×2560 grid, and 6 levels of refinement. Starting with a 20×20 grid, the number of cells per dimension was doubled until a 640×640 grid was reached. Visualizations of the solution density on the 20×20 grid, as well as the spatially resolved absolute error compared to the reference solution, are presented in Figure 8. The quantities for the 640×640 grid are presented in Figure 9. Additionally, the l^1 error in the density for each grid and a table of the order of accuracy is presented in Figure 10. The results show that our implementation exhibits the expected order of accuracy for this case. While results are only presented for the density, the same analysis was performed for all solution variables with consistently accurate results.

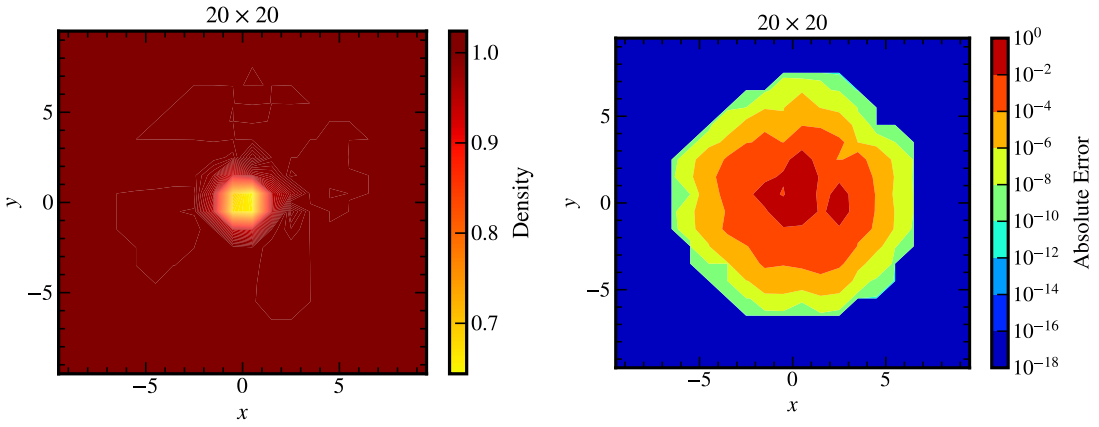

(a) *Reconstructed Density*

(b) *Absolute ℓ^1 Error*

Figure 8: *Reconstructed Density (ρ) and Error,* 20×20 *Grid, 2D Smooth Isentropic Unsteady Vortex*

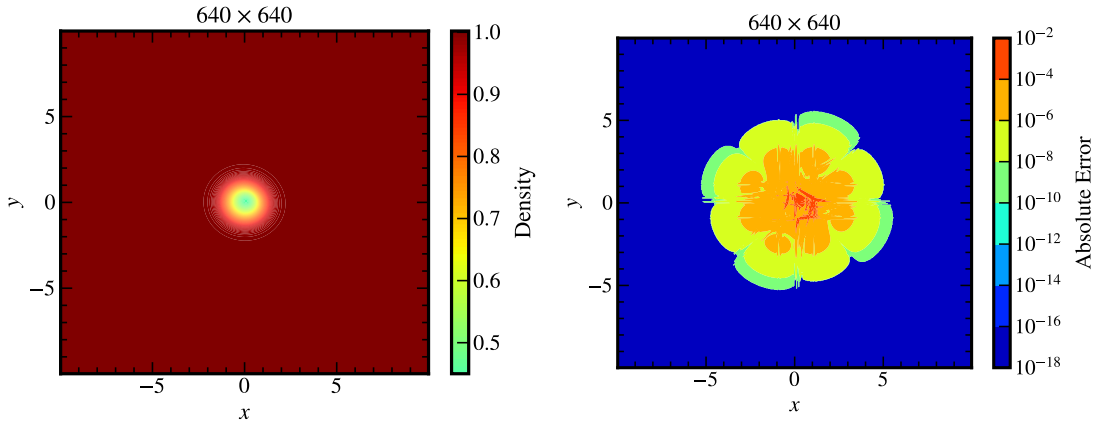

(a) *Reconstructed Density*

(b) *Absolute ℓ^1 Error*

Figure 9: *Reconstructed Density (ρ) and Error,* 640×640 *Grid, 2D Smooth Isentropic Unsteady Vortex*

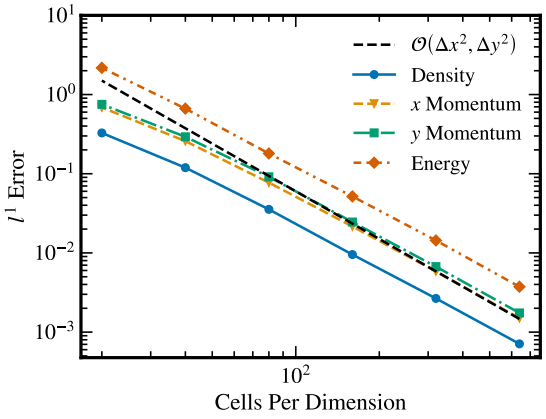

(a)

Grid	l^1 Errors	Rate
20×20	3.2743×10^{-1}	-
40×40	1.1931×10^{-1}	1.46
80×80	3.5483×10^{-2}	1.75
160×160	9.5349×10^{-3}	1.90
320×320	2.6629×10^{-3}	1.84
640×640	7.1048×10^{-4}	1.91

(b) *Convergence Rate - 2D Smooth Isentropic Unsteady Vortex*

Figure 10: *Smooth Isentropic Unsteady Vortex Errors*

6 Conclusion

In this report, we reviewed the classic Godunov central scheme in one spatial dimension, as well as its extension to the central-upwind formulation. We presented the central-upwind scheme in both its fully discrete and (conservative) semidiscrete forms, and discussed some of its underlying properties. In particular, we proved a result specifying a case in which the semidiscrete scheme is TVD. We concluded this background discussion with an outline of the derivation of the 2-D version of the scheme, also in semidiscrete form.

Using these results, we conducted several numerical experiments in both in one and two spatial dimensions. We used the 1-D version of the scheme to solve Burgers' equation supplied with a smooth initial

condition, as well as Euler's equations of gas dynamics with both smooth and non-smooth initial data. Correct orders of accuracy were observed across all three of these experiments, and the computed solutions matched all analytic/reference solutions available. Furthermore, we used the 2-D scheme to again solve Euler's equations, now supplied with a smooth isentropic unsteady vortex as an initial condition. A correct order of accuracy was also obtained, and the computed solutions produced reasonable errors when measured against a high-resolution reference.

References

[1] Shumo Cui et al. "Positivity-preserving new low-dissipation central-upwind schemes for compressible Euler equations". In: *Journal of Computational Physics* 538 (2025), p. 114189. ISSN: 0021-9991. DOI: https://doi.org/10.1016/j.jcp.2025.114189. URL: https://www.sciencedirect.com/science/article/pii/S0021999125004723.

[2] Bernd Einfeldt. "On Godunov-type methods for gas dynamics". In: *SIAM Journal on numerical analysis* 25.2 (1988), pp. 294–318.

[3] Ami Harten. "High resolution schemes for hyperbolic conservation laws". In: *Journal of computational physics* 135.2 (1997), pp. 260–278.

[4] Ami Harten et al. "Uniformly high order accurate essentially non-oscillatory schemes, III". In: *Journal of computational physics* 131.1 (1997), pp. 3–47.

[5] Alexander Kurganov, Sebastian Noelle, and Guergana Petrova. "Semidiscrete central-upwind schemes for hyperbolic conservation laws and Hamilton–Jacobi equations". In: *SIAM Journal on Scientific Computing* 23.3 (2001), pp. 707–740.

[6] Alexander Kurganov and Eitan Tadmor. "New high-resolution central schemes for nonlinear conservation laws and convection–diffusion equations". In: *Journal of computational physics* 160.1 (2000), pp. 241–282.

[7] Doron Levy, Gabriella Puppo, and Giovanni Russo. "A third order central WENO scheme for 2D conservation laws". In: *Applied Numerical Mathematics* 33.1-4 (2000), pp. 415–421.

[8] Doron Levy, Gabriella Puppo, and Giovanni Russo. "Compact central WENO schemes for multidimensional conservation laws". In: *SIAM Journal on Scientific Computing* 22.2 (2000), pp. 656–672.

[9] Lorenzo Micalizzi and Eleuterio Toro. *FORCE-α Numerical Fluxes within the Arbitrary High Order Semidiscrete WENO-DeC Framework: A Competitive Alternative to Upwind Fluxes*. 2025. arXiv: 2512.21306 [math.NA]. URL: https://arxiv.org/abs/2512.21306.

[10] Lorenzo Micalizzi and Eleuterio F Toro. "Impact of numerical fluxes on high order semidiscrete WENO-DeC finite volume schemes". In: *arXiv preprint arXiv:2411.07422* (2024).

[11] Eitan Tadmor. "Convenient Total Variation Diminishing Conditions for Nonlinear Difference Schemes". In: *SIAM Journal on Numerical Analysis* 25.5 (1988), pp. 1002–1014. DOI: 10.1137/0725057. eprint: https://doi.org/10.1137/0725057. URL: https://doi.org/10.1137/0725057.